JACS
JOURNAL OF THE AMERICAN CHEMICAL SOCIETY
Article
pubs.acs.org/JACS

Bimetallic C–C Bond-Forming Reductive Elimination from Nickel

Hongwei Xu, Justin B. Diccianni, Joseph Katigbak, Chunhua Hu, Yingkai Zhang, and Tianning Diao*

Department of Chemistry, New York University, 100 Washington Square East, New York, New York 10003, United States

Supporting Information

ABSTRACT: Ni-catalyzed cross-coupling reactions have found important applications in organic synthesis. The fundamental characterization of the key steps in cross-coupling reactions, including C–C bond-forming reductive elimination, represents a significant challenge. Bimolecular pathways were invoked in early proposals, but the experimental evidence was limited. We present the preparation of well-defined (pyridine-pyrrolyl)Ni monomethyl and monophenyl complexes that allow the direct observation of bimolecular reductive elimination to generate ethane and biphenyl, respectively. The sp^3–sp^3 and sp^2–sp^2 couplings proceed via two distinct pathways. Oxidants promote the fast formation of Ni(III) from (pyridine-pyrrolyl)Ni-methyl, which dimerizes to afford a bimetallic Ni(III) intermediate. Our data are most consistent with the subsequent methyl coupling from the bimetallic Ni(III) to generate ethane as the rate-determining step. In contrast, the formation of biphenyl is facilitated by the coordination of a bidentate donor ligand.

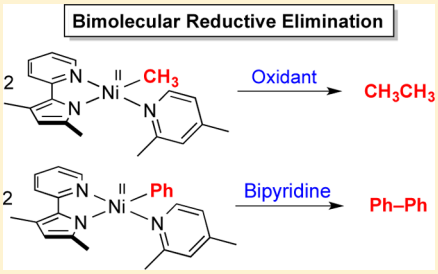

INTRODUCTION

Nickel complexes have emerged as appealing catalysts for cross-coupling reactions (eq 1).[1] While contemporary Ni catalysts

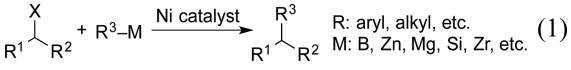

(1)

employing chelating ligands have started to solve important problems in organic synthesis,[2] catalyst design will benefit from advanced understanding of the reaction mechanisms to achieve more widespread utility.[3,4] The diversity of pathways, depending on the ligand framework, highlights the challenges associated with characterizing the mechanism for Ni-catalyzed cross-coupling reactions. The two prevailing mechanisms include the Pd-like "closed-shell" redox pathway via Ni(0)/Ni(II) intermediates[5] and the "open-shell" pathway featuring Ni(I)/Ni(III) intermediates.[4,6]

In parallel with catalytic studies, historical and contemporary efforts have focused on stoichiometric characterization of the fundamental steps of nickel-mediated C–C bond coupling. Several Ni(II) and Ni(III) systems have been identified to undergo reductive elimination,[6,7] whereas C–C bond formation from isolated Ni(IV) has just been reported recently.[8] Reductive elimination engaging two metal centers has been determined to promote C–C coupling with Pd and Pt complexes,[9] but such a bimetallic mechanism with Ni has seldom been considered.[10] Yamamoto observed transmetalation between two Ni(II) intermediates prior to a "closed-shell" reductive elimination of biphenyl from Ni(II) to Ni(0) (Scheme 1A).[7a−d] In contrast, early proposals by Kochi and Hegedus described a group transfer between Ni(III) and Ni(II) as the key step, followed by reductive elimination from the Ni(III) intermediate (Scheme 1B).[6,11] This "open-shell" transmetalation was supported by minimal experimental evidence.[12] In light of the fundamental interest and potential applications of bimolecular mechanisms in Ni catalysis, herein we present the direct observation of two distinct bimetallic pathways for Ni-mediated sp^3–sp^3 and sp^2–sp^2 C–C coupling. Spectroscopic and kinetic studies, in combination with DFT calculations, provide evidence for high-valent Ni intermediates. Our discovery of new bimetallic mechanisms for Ni-mediated C–C bond formation provides valuable insight for catalyst design in cross-coupling reactions.

Scheme 1. Proposed Bimetallic Pathways for Ni-Mediated C–C Bond Formation

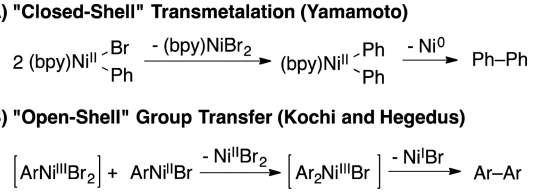

RESULTS AND DISCUSSION

Synthesis of Monomethyl and Monophenyl Ni Complexes. LX-type bidentate ligands are beneficial to Ni-catalyzed cross-coupling reactions,[13] but fundamental understanding of the ligand effect on C–C bond formation has been limited by the challenges associated with isolating Ni-carbyl intermediates.[14] We prepared (py-^{Me}pyrr)Ni(acac), **1** (py-^{Me}pyrr = 3,5-dimethyl-2-(2-pyridyl)pyrrole, acac = acetylacetonate), which underwent methylation and phenylation with Grignard reagents to afford *cis* and *trans* mixtures of (py-^{Me}pyrr)Ni(CH_3)(lut) (**2**) and (py-^{Me}pyrr)Ni(Ph)(lut) (**3**) (lut = 2,4-lutidine) (Scheme 2). The *cis*- and *trans*-isomers of **2** cocrystallized into a highly disordered packing (Figure S1(B)).

Received: January 1, 2016
Published: March 22, 2016

DOI: 10.1021/jacs.6b00016
J. Am. Chem. Soc. 2016, 138, 4779–4786

Scheme 2. Syntheses of (py-^{Me}pyrr)Ni Complexes

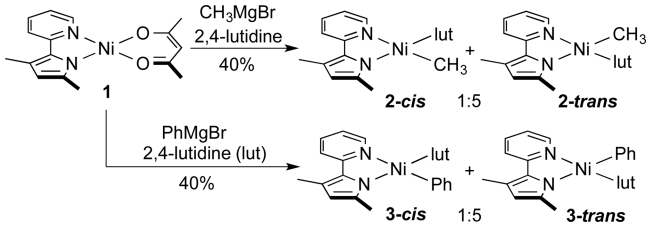

Our effort to crystalize **3** was not successful, so we prepared the alternative (py-^{Ph}pyrr)Ni(acac) (**7**) and (py-^{Ph}pyrr)Ni(Ph)(lut) (**8**). Single-crystal X-ray diffraction established a square planar geometry for **2** and **8** (Figures S1 and S2). This geometry implies a low-spin state for Ni and is consistent with the observed diamagnetic ^{1}H NMR spectra. In solution, the assignments of *cis*- and *trans*-isomers were confirmed by NOESY and COSY experiments (Figure S4). The *cis*/*trans* ratio remained constant over time, indicating that the preference for the *trans* geometry was a thermodynamic effect.[15] In the following studies, the isomers were not separated, but used as a mixture.

Oxidant-Promoted Ethane Formation. The isolation of **2** has allowed us to carry out fundamental studies on C−C bond formation from the well-defined monomethyl complex. We initiated our study by evaluating **2** under Yamamoto conditions, where transmetalation followed by biphenyl coupling was reported for (bpy)Ni(Ph)(Br) (bpy = bipyridine) in dimethylformamide (DMF).[7c] In contrast to this precedent, **2** remained stable in DMF-d_7 and C_6D_6 (Table 1, entries 1 and 2). We continued to explore the effect of external donor ligands and oxidants. Immediate decomposition of **2** to CH_4 was observed in the presence of 5 equiv of bpy (entry 3).[16] Addition of CH_3I to **2** resulted in minor conversion upon heating (entry 4). Introducing O_2 to **2** immediately furnished ethane in 19% yield (maximum theoretical yield = 50%) (entry 5).[17] The yield of ethane was increased to 43% with I_2 as the oxidant, with concomitant formation of 10% CH_3I (entry 6). Addition of *N*-bromosuccinimide (NBS) also led to high yield of ethane (entry 7). Notably, no methane was observed under these oxidative conditions.

Table 1. Formation of Ethane from 2

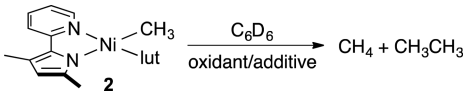

entry	oxidant or additive	temp (°C)	time (h)	yield (%)[a] CH_4	yield (%)[a] CH_3CH_3
1[b]	none	22	12	0	0
2	none	50	4	0	0
3	bpy (5 equiv)	50	4	60	trace
4	CH_3I (1 equiv)	50	4	4	4
5	O_2 (5 equiv)	22	0.1	0	19 ± 2
6	**I_2 (0.5 equiv)**	**22**	**0.1**	**0**	**43**[c]
7	**NBS (1 equiv)**	**22**	**0.1**	**< 1**	**45**[d]

[a]Internal standard = hexamethyldisiloxane (TMS_2O). The yield of ethane is based on molar concentration (the maximum yield is 50%). Methane and ethane in the gas phase are calculated using Henry's law. [b]In DMF-d_7. [c]CH_3I was observed in 10% yield. [d]CH_3Br was observed in 2% yield.

The selective ethane formation from **2** under oxidative conditions provided preliminary support for a bimolecular reductive elimination process. We continued our investigation to obtain further evidence for a bimolecular pathway. A crossover experiment was performed in which a mixture of **2** and **2-d_3** in a 1:1 ratio reacted with I_2 to generate a mixture of CH_3CH_3, CH_3CD_3, and CD_3CD_3 in a statistical distribution (eq 2). The ratio of ethane to CH_3I exhibited a linear

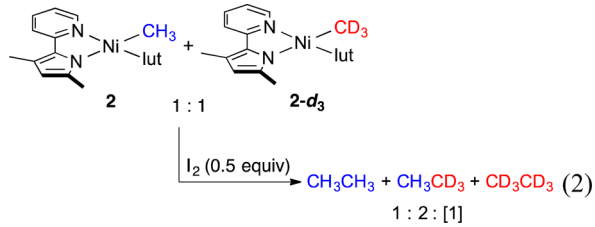

dependence on [**2**] with a positive slope (Figure 1). The influence of [**2**] on the product distribution reflects the requirement for two molecules of **2** to form ethane, whereas the formation of CH_3I is unimolecular in **2**.

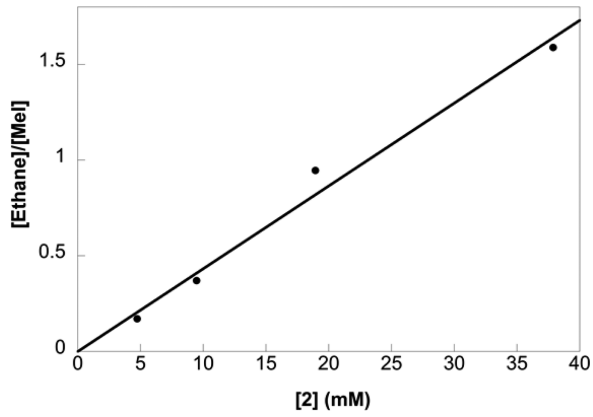

Figure 1. Dependence of [ethane]/[CH_3I] ratio on [**2**]. Reaction conditions: [**2**] = 5−40 mM, [I_2] = 20 mM, C_6D_6 = 0.6 mL, 22 °C, 1 h. Internal standard = TMS_2O. Estimated standard deviation for individual points: ≤5%.

Experimental and Theoretical Characterization of Intermediates. *A. Spectroscopic Data.* Our subsequent spectroscopic studies on I_2-promoted ethane formation from **2** provided structural information on the Ni intermediates and shed some light on the reaction mechanism. The cyclic voltammetry (CV) of **2** exhibited two irreversible oxidation waves at 12 and 411 mV (vs Fc/Fc^+) (Figure S5). In a liquid N_2 filled cold well, **2** and I_2 were mixed and the reaction mixture was immediately analyzed by electron paramagnetic resonance (EPR) spectroscopy. The EPR spectrum displayed a single species of an $S = 1/2$ state with a 1:1:1 superhyperfine splitting (Figure 2, red).[18] To determine the lifetime of this intermediate, we allowed the mixture to react at −20 °C for 10 min and examined it by EPR spectroscopy. The signal corresponding to the intermediate decayed to zero. When NBS was used to replace I_2 as the oxidant, an analogous intermediate was observed (Figure 2, black). The features and splitting patterns for the two intermediates, generated from I_2 and NBS (red and black, respectively), are similar, but the *g* values are slightly different, reflecting two distinct complexes with a similar structure.

DOI: 10.1021/jacs.6b00016
J. Am. Chem. Soc. 2016, 138, 4779−4786

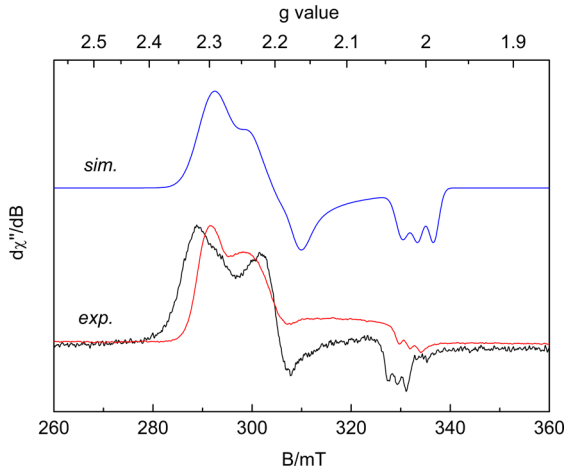

Figure 2. X-band EPR spectra of the intermediate generated from the reaction of **2** with I_2 (red) and the reaction of **2** with NBS (black) recorded in toluene glass at 10 K. The blue spectrum (top) is the simulation of the red spectrum. Spectroscopic parameters: g_x = 2.20, g_y = 2.14, g_z = 2.03, A_{xx} = 7.7 MHz, A_{yy} = 63 MHz, A_{zz} = 55 MHz. Microwave frequency = 9.380 GHz, power = 0.25 mW, modulation amplitude = 1 mT/100 kHz.

The short-lived Ni(III) intermediate detected by EPR spectroscopy prompted us to explore its structure by DFT calculations. Geometry optimization of possible Ni(III) intermediates converged to (py-^{Me}pyrr)Ni^{III}(CH_3)(I)(lut) (**4**) (Figure 3). This structure features a square pyramidal geometry

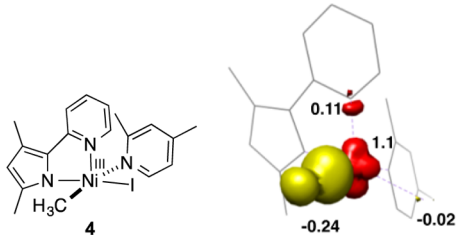

Figure 3. Structures and Mulliken spin-density plots of **4** obtained from DFT calculations.

with pyridine in the axial position and iodide *trans* to pyrrole. The spin-density plot reveals a Ni-centered radical strongly coupled with the N-atom of pyridine, whereas its couplings with pyrrole and lutidine are minor. The EPR parameters of **4** were calculated using the ORCA package,[19] and the computational g values and A_{iso} reproduced the experimental spectra shown in Figure 2 (Table S1).

Variable-temperature NMR experiments allowed us to identify the diamagnetic intermediates. In a liquid nitrogen-filled cold well, upon injection of I_2, **2** rapidly evolved into a diamagnetic intermediate with the concomitant formation of CH_3I in 10% yield and minor paramagnetic species (Figure S7A). While the complete conversion of this intermediate to ethane was fast at 22 °C (Figure S7B), the intermediate was stable on the NMR time scale at −20 °C (Figure S8). Multiple singlet resonances in the upfield region between 2.0 and 3.0 ppm are accompanied by several aromatic protons between 5.5 and 7.0 ppm. COSY experiments elucidate that a number of resonances overlap with the residual toluene solvent signals (Figure S9). To determine the identity of this intermediate and assign the spectrum, we prepared deuterium labeled (py-^{Me}pyrr)Ni-methyl complexes, **2-d_3**, **2-d_1**, and **2-d_7** (Figure 4). Complex **2-d_7** is a mixture of isotopologues and

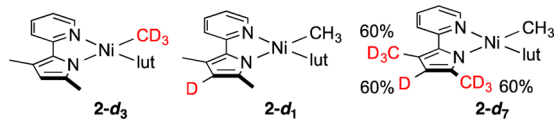

Figure 4. Deuterium-labeled **2** for structure assignment of the diamagnetic intermediate.

isotopomers. The overall deuterium incorporation in **2-d_7** is 60% at each position. When **2-d_3** was treated with I_2, four signals at 3.00, 2.94, 2.91, and 2.85 ppm disappeared (Figure 5A). HSQC experiments revealed that the carbon chemical shifts corresponding to these proton resonances were between 26.00 and 29.00 ppm (Figure S10). The concentration of these four proton resonances, in combination with CH_3I, accounted for 95% of the Ni-CH_3 from the starting **2**. Moreover, the overall integration of these four signals is half the overall integration of eight singlet peaks between 2.30 and 2.60 ppm (Figure S8). The reaction of **2-d_1** led to the disappearance of two singlet ^{1}H resonances at 6.14 and 6.17 ppm, while all other resonances remained (Figure 5B). When **2-d_7** was submitted to the reaction conditions, all eight singlet resonances between 2.30 and 2.60 ppm diminished with small residuals due to the incomplete deuterium incorporation in **2-d_7** (Figure 5C).

The ^{1}H NMR resonances corresponding to the diamagnetic intermediate gradually decrease at −20 °C, while a singlet resonance at 0.820 ppm, corresponding to ethane, increases. The concentration of CH_3I remains constant. We were able to monitor the decay of the intermediate and formation of ethane over 3−4 h. The concentration of the Ni−CH_3 at 3.00 ppm exhibits an exponential decay (Figure 6A).[20] The concentration of this species, however, only accounts for a fraction of the ethane generated. When all four Ni-CH_3 resonances identified in Figure 5A at 3.00, 2.94, 2.91, and 2.85 ppm are integrated, half of the total concentration fit to a first-order kinetic model (Figure 6B). The same model accommodates the concentration of ethane.[21] Other models, including second-order kinetics, were fully considered but failed to fit the experimental data. When the conversion of the intermediate to ethane was complete, the resulting Ni species were NMR silent (Figure S7B). The EPR spectrum revealed the absence of any radical species. Independently prepared (py-pyrr)$_2$Ni^{II} and the comparison of the spectra revealed that (py-pyrr)$_2$Ni^{II} is absent from the reaction (Scheme 3, cf. Figures S11 and S12). Alternatively, tetrahedral (py-pyrr)Ni-iodides are possible products (Scheme 3). Our attempts to prepare (py-pyrr)Ni iodides via multiple methods were unsuccessful, consistent with previous reports by Caulton and coworkers.[14b,22]

B. Structural Assignment of Intermediate 4. The irreversible CV of **2** at 12 and 411 mV (vs Fc/Fc$^+$) suggests that the high-valent Ni species generated from electrochemical oxidation are unstable. Nevertheless, the data provide an estimation of the oxidation potentials for Ni(II)/Ni(III) and Ni(III)/Ni(IV) transitions. Previous reports indicate that the oxidation potential of I_2 is 140 mV (vs Fc/Fc$^+$),[23] implying that I_2 is suitable for oxidizing **2** to Ni(III) instead of Ni(IV). This analysis agrees with previous experimental and computational studies on the oxidation of Ni(II) to Ni(III) by Br_2.[24] The EPR experiments provide further support for the oxidation of **2** to a Ni(III) intermediate upon addition of I_2. Replacing I_2 with NBS

DOI: 10.1021/jacs.6b00016
J. Am. Chem. Soc. 2016, 138, 4779−4786

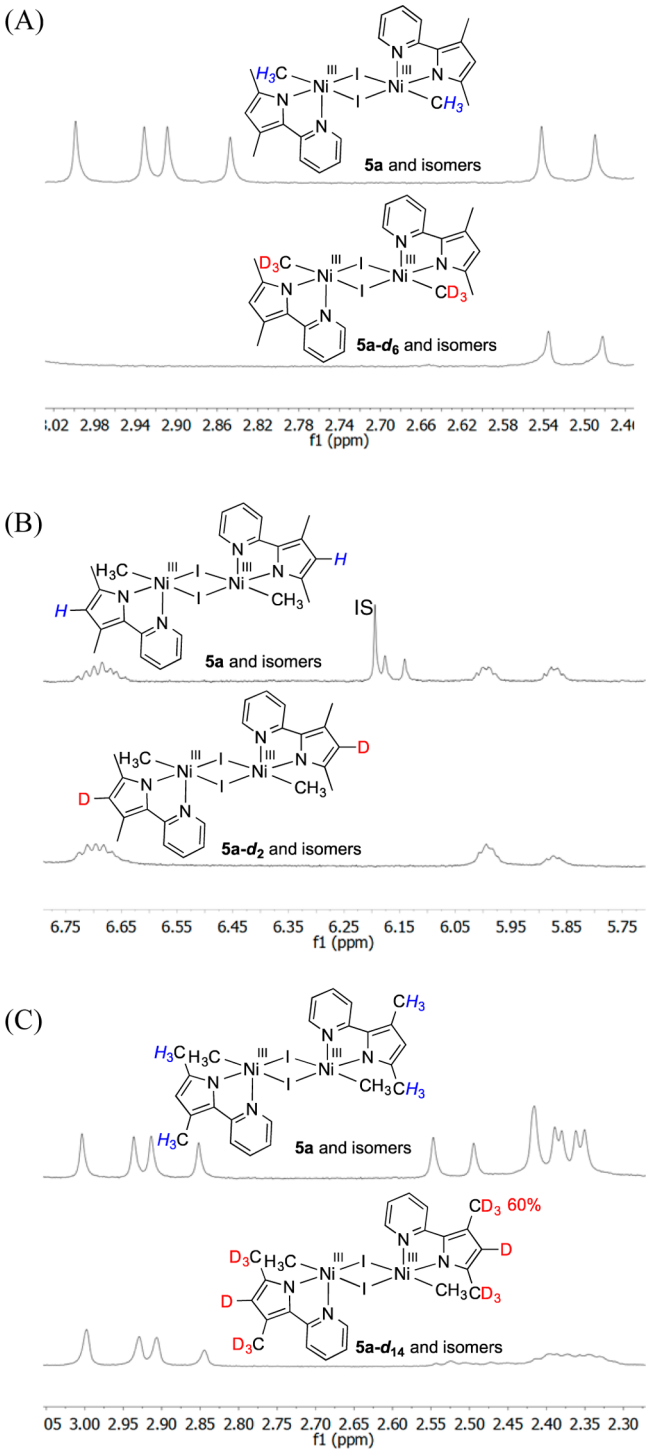

Figure 5. Comparison of the ^{1}H NMR spectra of the intermediate generated from I_2 reacting with protio and deuterio (py-pyrr)Ni-methyl complexes **2**-d_3 (A), **2**-d_1 (B), and **2**-d_7 (C). Reaction conditions: [**2**] = 16 mM, [I_2] = 16 mM, toluene-d_8 = 0.65 mL, −20 °C. Internal standard (IS) = 1,3,5-trimethoxybenzene.

leads to a minor shift of the *g* values while the overall shape of the EPR signal is unchanged. This observation suggests that the Ni(III) intermediate possesses a halide ligand.[25] DFT calculations allow us to propose (py-^{Me}pyrr)Ni^{III}(I)(CH_3)(lut) (**4**) as the possible structure (Figure 3). The square pyramidal geometry is consistent with a Ni(III)-halide previously isolated by van Koten.[25b,d] The calculated EPR parameters for **4** are in good agreement with the experimental values (Table S1). The observed 1:1:1 superhyperfine splitting is due to the strong coupling of the unpaired electron on Ni with the N of pyridine (I = 1) in the axial position. The lifetime of **4** at −20 °C is short, as its EPR signal has completely decayed after 10 min.

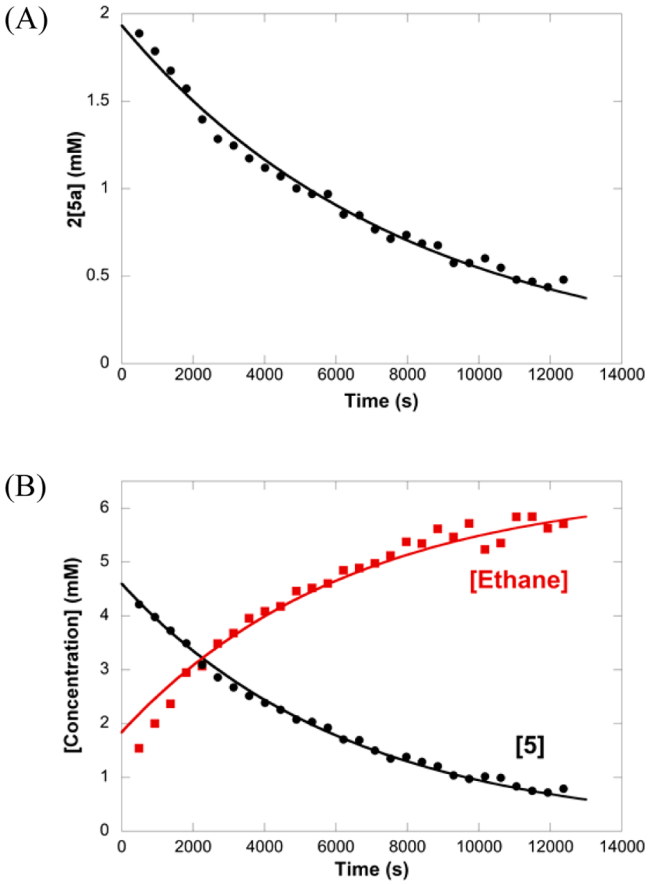

Figure 6. Reaction time courses for the consumption of the Ni−CH_3 resonance at 3.00 ppm (2[**5a**]) (A) and the conversion of **5** to ethane (B). The concentration of **5** ([**5**] = [**5a**] + [**5b**] + [**5c**]) was calculated by dividing the total concentration of four Ni-CH_3 resonances at 3.0, 2.94, 2.91, and 2.85 ppm by 2 (see discussions below). Reaction conditions: $[\mathbf{2}]_0$ = 17 mM, $[I_2]_0$ = 15 mM, toluene-d_8 = 0.65 mL, −20 °C. Internal standard = 1,3,5-trimethoxybenzene.

Scheme 3. Proposed Ni Products from the Reaction of 2 with I_2

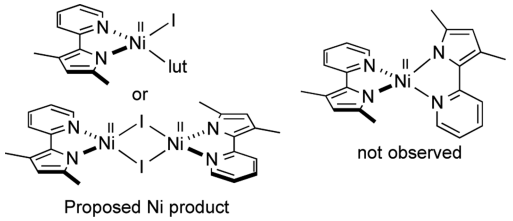

C. Structural Assignment of Intermediate **5**. Low-temperature ^{1}H NMR studies reveal a diamagnetic intermediate **5** with a lifetime of 3−4 h at −20 °C. The assignment of the peaks is facilitated by the deuterium labeling studies, 2D NMR experiments, and literature precedents. The reaction of **2**-d_3 leads to the disappearance of four peaks at 3.00, 2.94, 2.91, and 2.85 ppm (Figure 5A), suggesting four Ni−CH_3 resonances exist for intermediate **5**. Consistently, the total concentration of these methyl groups, along with the small amount of CH_3I

DOI: 10.1021/jacs.6b00016
J. Am. Chem. Soc. 2016, 138, 4779−4786

byproduct, accounts for 95% of the starting Ni-CH_3 from **2**. The concentration of each individual Ni−CH_3 resonance (3.00 ppm, for instance) undergoes first-order decay at −20 °C (Figure 6A). Half of the overall concentration of the four Ni−CH_3 resonances fit to a first-order kinetic model, which accounts for the formation of ethane (Figure 6B). These kinetic data are consistent with two Ni−CH_3 groups in each molecule of **5**, which couple in an intramolecular fashion to generate ethane.

The ^{1}H chemical shifts of Ni−CH_3 and the ^{13}C resonances of the corresponding Ni−CH_3 are unusually downfield for methyl resonances attached to metals (Figures 5A and S10), implying an electron-deficient Ni center. Previous reports of high-valent Ni complexes display an analogous trend (Scheme 4).[8,26] The

Scheme 4. Reported ^{1}H Chemical Shifts of High-Valent Ni Complexes

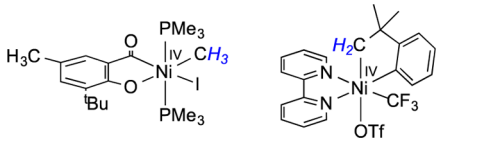

δ(dioxane-d_8) 1.16 ppm
Klein, **1994**

δ(CD_3CN) 4.67 and 3.75 ppm
Sanford, **2015**

experiment with **2**-d_7 reveals that all eight methyl peaks between 2.30 and 2.60 ppm belong to the py-pyrr ligand (Figure 5C). The integrations suggest that the ratio of Ni−CH_3/py-pyrr is 1:1. These considerations, coupled with the kinetic data, lead us to propose the dimeric [(py-pyrr)-$Ni^{III}(CH_3)(\mu$-I)]$_2$ as the structure of intermediate **5** (Scheme 5). The diamagnetic property of **5** arises from the antiferromagnetic coupling of low-spin Ni(III) (d^7, S = 1/2) centers.[27] The integrations of the ^{1}H NMR resonances and 2D NMR experiments suggest that three isomers exist. Duplicate experiments show different ratios of the isomers, suggesting a distribution originating from a kinetic effect instead of thermodynamic equilibrium. DFT calculations on possible stereoisomers converged to two symmetric structures that have the lowest energy, **5a** and **5b** (Scheme 5). The Ni centers favor a square pyramidal geometry with pyridine occupying the axial position. NMR data determined that the third isomer has two inequivalent Ni−CH_3 and two sets of py-pyrr ligands. DFT calculations converged to **5c**, in which one Ni adapts a square pyramidal geometry and the other is trigonal bipyramidal with an iodide and a methyl located at the axial position (Scheme 5). The assignment of the ^{1}H resonances for each isomer is presented in Scheme 5. The assignments for **5c** in brackets are arbitrary, since we do not have a way to distinguish between the two inequivalent py-pyrr ligands. The missing resonances are attributed to peaks underneath the residual toluene solvent.

The calculated chemical shifts of Ni−CH_3 in each isomer are 3.75, 3.57, 2.87, and 2.77 ppm, respectively, in agreement with the experimental values.

Alternatively, Ni(IV)-dimethyl complexes were considered as the structure of **5**, and could be ruled out by our data. (Py-pyrr)$Ni^{IV}(CH_3)_2$(lut)(I) **5d** is a possible intermediate (Scheme 6). The ratio of Ni−CH_3/py-pyrr for **5d** is 2:1, inconsistent

Scheme 6. Ni(IV) Complexes Ruled Out as the Structure of 5 and the Corresponding Ni−CH_3 ^{1}H NMR Chemical Shifts Predicted by DFT Calculations

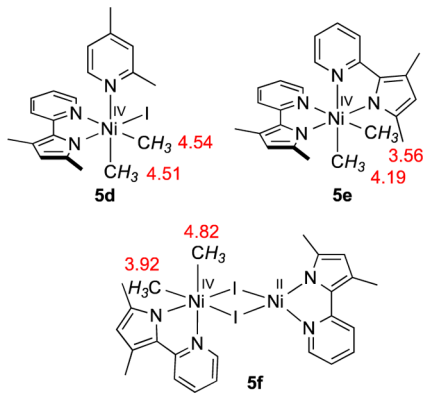

with the observed Ni−CH_3/py-pyrr ratio of 1:1 by NMR labeling studies. (Py-pyrr)$_2Ni^{IV}(CH_3)_2$ **5e** would fit the kinetic and NMR data. The reductive elimination from **5e** to form ethane is expected to generate (py-pyrr)$_2Ni^{II}$ as the resulting Ni species. The lack of (py-pyrr)$_2Ni^{II}$ after the reaction suggests that **5e** is absent (Scheme 3, cf. Figures S11 and S12). In addition, the formation of **5e** requires the transfer of the py-pyrr ligand and methyl from one molecule of **4** to another. This process is highly unlikely. The mixed-valent (py-pyrr)-$Ni^{IV}(CH_3)_2(\mu$-I)$_2Ni^{II}$(py-pyrr) **5f** would fit the kinetic data. However, the py-pyrr ligands in any stereoisomers of **5f** are inequivalent, inconsistent with the symmetry of the three isomers determined by ^{1}H NMR spectroscopy. Moreover, we performed DFT calculations on **5f**, which converged to an octahedral Ni(IV) bridged with a tetrahedral Ni(II). The tetrahedral Ni(II) is high-spin, contradictory to the observed diamagnetic NMR spectrum. The calculated Ni−CH_3 ^{1}H NMR chemical shifts are significantly more downfield compared to the experimental values.

Mechanism of Oxidant-Promoted Ethane Formation. In the studies presented above, we explored and characterized the C−C bond formation process from (py-pyrr)Ni monomethyl complex **2**. The lack of reactivity of **2** in DMF contradicts Yamamoto's "closed-shell" pathway.[7] The absence of ethane in the presence of CH_3I reveals a pathway distinct from simple nucleophilic substitution[28] or oxidation of Ni(II)

Scheme 5. Proposed Structures for Intermediate 5 and Assignments of ^{1}H NMR Resonances

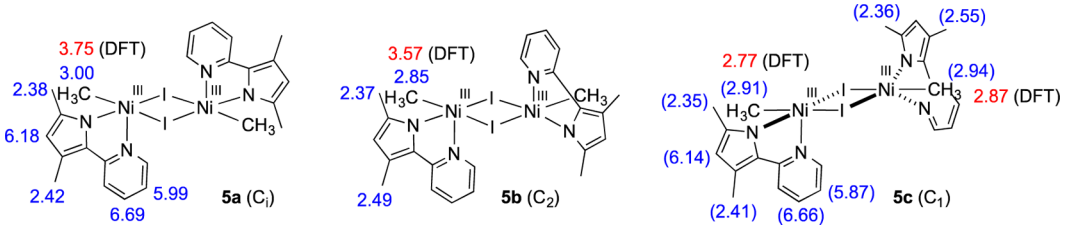

DOI: 10.1021/jacs.6b00016
J. Am. Chem. Soc. 2016, 138, 4779−4786

Scheme 7. Proposed Mechanism for I_2-Promoted Reductive Elimination of Ethane

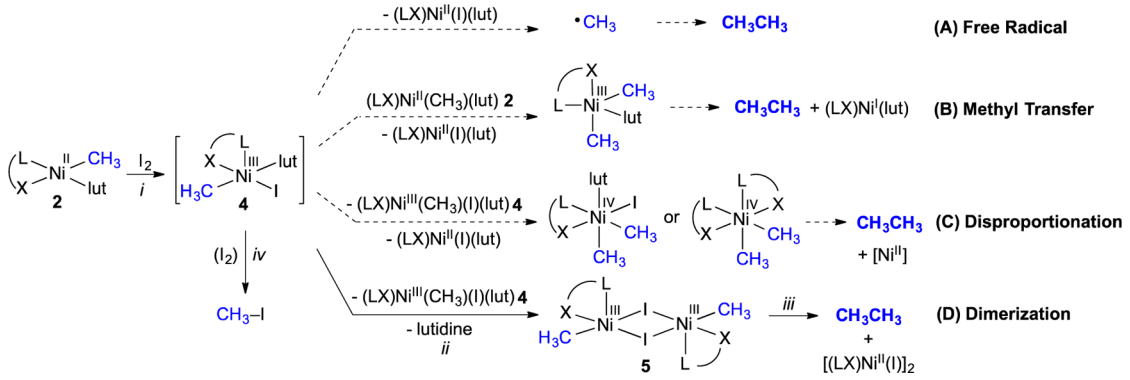

by CH_3I.[2a] Instead, **2** undergoes reductive elimination to generate ethane in the presence of oxidants. This reaction is highly selective, since methane is absent from the reaction. The I_2-promoted ethane formation is bimolecular, evident in the crossover experiment and the increased [ethane]/[CH_3I] ratio as a function of [**2**].

On the basis of the structural assignment of the intermediates above, we propose the mechanism for I_2-promoted ethane formation (Scheme 7). The process is initiated by the oxidation of **2** to afford a Ni(III) intermediate, assigned as (py-^{Me}pyrr)-Ni^{III}(I)(lut)(CH_3) (**4**) (step *i*) (Scheme 7). Intermediate **4** has a short lifetime and rapidly undergoes further conversion. Four possible pathways are considered for the subsequent ethane formation. In the free radical pathway (Scheme 7, pathway A), **4** undergoes a Ni–C bond homolysis to eject a methyl radical, which dimerizes to generate ethane. This pathway is inconsistent with the absence of methane after the reaction, since methane is an expected product from the ejection of a methyl radical.[29] Moreover, monitoring the reaction by ^{1}H NMR spectroscopy clearly reveals the conversion of organometallic Ni–CH_3 intermediates to ethane. The radical mechanism is inconsistent with the clean first-order kinetics. In comparison, the reaction of **2** with bpy is speculated to form a methyl radical, which results in methane as the major product (Table 1, entry 3) (see below for further discussion about ligand-promoted radical ejection).

An alternative mechanism involves a methyl transfer from **4** to **2** to afford a Ni(III)-dimethyl intermediate (pathway B). This pathway is reminiscent of Kochi's and Hegedus's proposals.[6] The rapid decay of paramagnetic intermediate **4** into EPR silent species is contradictory to a Ni(III)-dimethyl intermediate. Instead, a diamagnetic intermediate **5** converts to ethane over 3–4 h at −20 °C. Pd(III) has been reported to undergo disproportionation to afford Pd(IV), followed by reductive elimination to form ethane.[9a] We evaluated the analogous pathway (pathway C). The possible Ni(IV) complexes, which could arise from disproportionation, can be ruled out as the structure of intermediate **5** based on the direct and circumstantial evidence presented above (Scheme 6).

The NMR and kinetic data fit well to [(py-pyrr)Ni^{III}(CH_3)-(μ-I)]$_2$ **5**, which is generated from the dissociation of 2,4-lutidine from **4** (step *ii*, pathway D). The reductive elimination from **5** to furnish ethane is first-order, and is the rate-determining step (step *iii*). The precise transition state for the C–C bond formation is unknown. We speculate that the dissociation of the μ-iodide occurs prior to methyl coupling. The lack of S = 1/2 species after the reaction is evident from the EPR studies, which implies a Ni(II) as the resulting Ni product. The broad NMR signals suggest that the resulting Ni(II) is high-spin. The competing reductive elimination of CH_3I from **4** (step *vi*) takes place in parallel with the dimerization (step *ii*). Once **5** is formed, the bridging μ-iodide inhibits CH_3I reductive elimination, consistent with the constant [CH_3I] after the initial period of the reaction. The favorable formation of ethane relative to CH_3I is a result of the fast dimerization (step *ii*).

Donor Ligand-Promoted Bimolecular Biphenyl Formation. (Py-^{Me}pyrr)Ni(Ph)(lut), **3**, underwent C–C bond formation via a different pathway, relative to **2**. Complex **3** remained intact in DMF-d_7 and C_6D_6 (Table 2, entries 1 and 2). Addition of bpy afforded biphenyl in 49% yield upon heating (maximum theoretical yield = 50%) (entry 3). Neither addition of CH_3I (entry 4) nor O_2 (entry 5) to **3** afford biphenyl or toluene. Repeating the experiment in toluene-d_8 resulted in the absence of benzene and phenol. Addition of I_2 resulted in PhI in high yield (entry 6).

Table 2. Formation of Biphenyl from 3

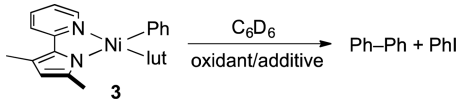

3

				yield (%)[a]		
entry	oxidant or additive	temp (°C)	time (h)	Ph–Ph	PhI	$PhCH_3$
1[b]	none	22	12	0		
2	none	50	4	trace		
3	**bpy (5 equiv)**	**50**	**4**	**49**		
4	CH_3I (1 equiv)	50	4	0		0
5	O_2 (5 equiv)	22	0.1	0		
6	I_2 (0.5 equiv)	22	0.1	0	97	

[a]TMS_2O was added as the internal standard. The yield of biphenyl is based on molar concentration (the maximum yield is 50%). [b]In DMF-d_7.

The high yield of biphenyl in the presence of bpy prompted us to undertake further characterization of the reaction pathway and the intermediate. The crossover experiment between **3** and (py-^{Me}pyrr)Ni(*p*-Tol)(lut) afforded a mixture of biphenyl, 4-phenyltoluene, and 4,4′-dimethylbiphenyl in a ratio comparable to the statistical distribution (eq 3). While 1 equiv of phenanthroline was capable of fully displacing lutidine from **3** to afford the penta-coordinated (py-^{Me}pyrr)Ni(Ph)(phen) **10** (Figure S3(B)), ligand substitution between **3** and bpy favored dissociation (eq 4). The equilibrium constant was determined

DOI: 10.1021/jacs.6b00016
J. Am. Chem. Soc. 2016, 138, 4779–4786

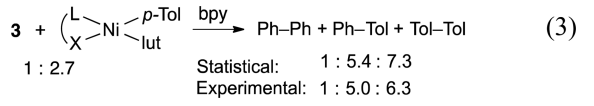

(3)

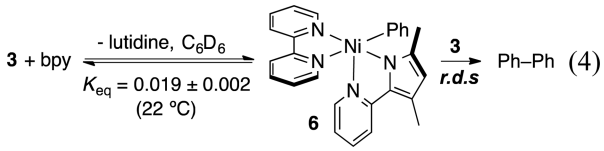

(4)

to be 0.019 ± 0.002 at 22 °C, by integrating the ^{1}H resonances of **3** and **6** in the presence of different concentrations of 2,4-lutidine. The full conversion of **3** to **6** was achieved by removing 2,4-lutidine under vacuum followed by re-dissolving in C_6D_6 five times. At 22 °C, **6** evolved biphenyl in full conversion after 2 h.

EPR analyses provided additional insight into the mechanism of this transformation. The reaction of (py-^{Me}pyrr)Ni^{II}(Me)(lut), **2**, with 1 equiv of (bpy)Ni^0(cod) (eq 5) exhibited a

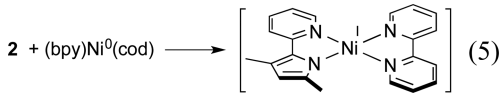

(5)

rhombic signal corresponding to an $S = 1/2$ Ni species at 50 K in toluene glass (Figure 7, red spectrum). An organic radical is

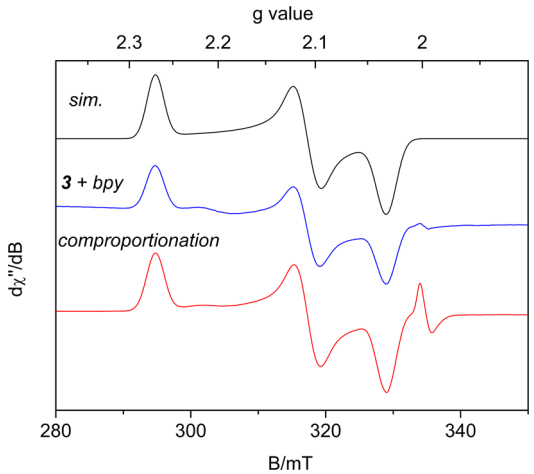

Figure 7. X-band EPR spectra recorded in toluene glass at 50 K for the reaction mixture of **3** with bpy (blue) and the comproportionation reaction (eq 5) (red). The black spectrum is the simulation of the red spectrum: $g_x = 2.27$, $g_y = 2.11$, $g_z = 2.04$, $A_{xx} = 3.7$ MHz, $A_{yy} = 26$ MHz, $A_{zz} = 8.5$ MHz.

present, which could result from the decomposition of Ni(I). This paramagnetic species is assigned to (py-^{Me}pyrr)Ni^I(bpy), generated in situ by the comproportionation of Ni(II) with Ni(0). The EPR spectrum of the reaction mixture of **3** with bpy displayed the same species (Figure 7, blue spectrum).

The statistical distribution of products from the crossover experiment (eq 3) provides crucial evidence for a bimolecular pathway for bpy-promoted biphenyl formation. Increasing the coordination number of a transition metal complex has been reported to trigger the ejection of alkyl/aryl radicals via steric interactions.[30] Free phenyl radicals are not involved here, since benzene is not an observed product. Instead, a phenyl group transfer from **6** to **3** can be proposed to generate a Ni(III)-diphenyl intermediate, which undergoes reductive elimination. This hypothesis is consistent with (py-^{Me}pyrr)Ni^I(bpy) as the resulting Ni species; however, other pathways cannot be ruled out. For example, bpy may bridge between two molecules of **3** to facilitate the bimolecular reductive elimination. Our ongoing efforts focus on elucidation of the precise role of bpy in this reaction by engaging in DFT calculations.

CONCLUSION

Collectively, we have established two bimolecular pathways for Ni-mediated C–C bond formation. The sp^3–sp^3 coupling of Ni–CH_3 to form ethane is initiated by oxidation to generate Ni(III), which dimerizes to afford the diamagnetic, bimetallic Ni(III)–CH_3 intermediate. The resulting Ni(III)–CH_3 dimer undergoes rate-determining reductive elimination to afford ethane (Scheme 7). The bimolecular pathway is verified by crossover experiments and the increased [ethane]/[CH_3I] ratio with increasing [Ni–CH_3]. The initial Ni(III) intermediate is characterized by EPR spectroscopy, and evidence for the bimetallic [Ni(III)–CH_3]$_2$ includes ^{1}H NMR experiments and kinetic studies. The experimental data are in good agreement with DFT calculations. Biphenyl formation, in contrast, is triggered by the coordination of a bidentate donor ligand (eq 4). While EPR characterization of the resulting Ni(I) species supports a phenyl transfer between two Ni(II) intermediates to generate a Ni(III)-diphenyl intermediate, the precise mechanism requires further investigation. These two bimetallic reductive elimination pathways presented here highlight the complexity of Ni-mediated C–C bond formation reactions. The elucidation of the bimolecular mechanism provides important insight for future design of active Ni catalysts for cross-coupling and homocoupling reactions.

ASSOCIATED CONTENT

Supporting Information

The Supporting Information is available free of charge on the ACS Publications website at DOI: 10.1021/jacs.6b00016.

Experimental procedures, additional discussions and figures, details of DFT calculations, NMR spectra, and crystallographic data, including Figures S1–S15 and Tables S1 and S2 (PDF)

X-ray crystallographic data for **1**, **2**, **7**–**10** (CIF)

AUTHOR INFORMATION

Corresponding Author

*diao@nyu.edu

Notes

The authors declare no competing financial interest.

ACKNOWLEDGMENTS

We thank Brian Schaefer, Valerie Schmidt, and Nadia Leonard (Chirik lab, Princeton University) for assistance in recording EPR spectra and Michelle Li for preparing the py-^{Ph}pyrr ligand. This work was supported by the NYU-MRSEC Program funded by National Science Foundation under award number DMR-1420073 and New York University.

REFERENCES

(1) For leading reviews of Ni-catalyzed cross-coupling reactions, see: (a) Netherton, M. R.; Fu, G. C. *Adv. Synth. Catal.* **2004**, *346*, 1525. (b) Frisch, A. C.; Beller, M. *Angew. Chem., Int. Ed.* **2005**, *44*, 674. (c) Tamaru, Y. *Modern Organonickel Chemistry*; Wiley-VCH:

DOI: 10.1021/jacs.6b00016
J. Am. Chem. Soc. 2016, 138, 4779–4786

Weinheim, 2005. (d) Rudolph, A.; Lautens, M. *Angew. Chem., Int. Ed.* **2009**, *48*, 2656. (e) Rosen, B. M.; Quasdorf, K. W.; Wilson, D. A.; Zhang, N.; Resmerita, A.-M.; Garg, N. K.; Percec, V. *Chem. Rev.* **2011**, *111*, 1346. (f) Jahn, U. In *Radicals in Synthesis III*; Heinrich, M., Gansäuer, A., Eds.; Springer: Berlin/Heidelberg, 2012; Vol. *320*, p 323. (g) Tasker, S. Z.; Standley, E. A.; Jamison, T. F. *Nature* **2014**, *509*, 299. (h) Su, B.; Cao, Z.-C.; Shi, Z.-J. *Acc. Chem. Res.* **2015**, *48*, 886. (i) Standley, E. A.; Tasker, S. Z.; Jensen, K. L.; Jamison, T. F. *Acc. Chem. Res.* **2015**, *48*, 1503. (j) Weix, D. J. *Acc. Chem. Res.* **2015**, *48*, 1767.

(2) For leading references, see: (a) Zhou, J.; Fu, G. C. *J. Am. Chem. Soc.* **2003**, *125*, 14726. (b) Vechorkin, O.; Proust, V.; Hu, X. *J. Am. Chem. Soc.* **2009**, *131*, 9756. (c) Everson, D. A.; Shrestha, R.; Weix, D. J. *J. Am. Chem. Soc.* **2010**, *132*, 920. (d) Ackerman, L. K. G.; Lovell, M. M.; Weix, D. J. *Nature* **2015**, *524*, 454.

(3) For a recent review, see: Hu, X. *Chem. Sci.* **2011**, *2*, 1867.

(4) For recent mechanistic studies of important systems, see: (a) Schley, N. D.; Fu, G. C. *J. Am. Chem. Soc.* **2014**, *136*, 16588. (b) Breitenfeld, J.; Ruiz, J.; Wodrich, M. D.; Hu, X. *J. Am. Chem. Soc.* **2013**, *135*, 12004. (c) Biswas, S.; Weix, D. J. *J. Am. Chem. Soc.* **2013**, *135*, 16192. (d) Breitenfeld, J.; Wodrich, M. D.; Hu, X. *Organometallics* **2014**, *33*, 5708.

(5) (a) Parshall, G. W. *J. Am. Chem. Soc.* **1974**, *96*, 2360. (b) Jin, L.; Zhang, H.; Li, P.; Sowa, J. R.; Lei, A. *J. Am. Chem. Soc.* **2009**, *131*, 9892.

(6) (a) Hegedus, L. S.; Miller, L. L. *J. Am. Chem. Soc.* **1975**, *97*, 459. (b) Tsou, T. T.; Kochi, J. K. *J. Am. Chem. Soc.* **1979**, *101*, 6319. (c) Tsou, T. T.; Kochi, J. K. *J. Am. Chem. Soc.* **1979**, *101*, 7547. (d) Hegedus, L. S.; Thompson, D. H. P. *J. Am. Chem. Soc.* **1985**, *107*, 5663.

(7) (a) Yamamoto, T.; Yamamoto, A.; Ikeda, S. *J. Am. Chem. Soc.* **1971**, *93*, 3350. (b) Komiya, S.; Abe, Y.; Yamamoto, A.; Yamamoto, T. *Organometallics* **1983**, *2*, 1466. (c) Yamamoto, T.; Wakabayashi, S.; Osakada, K. *J. Organomet. Chem.* **1992**, *428*, 223. (d) Yamamoto, T.; Abla, M.; Murakami, Y. *Bull. Chem. Soc. Jpn.* **2002**, *75*, 1997. (e) Anderson, T. J.; Jones, G. D.; Vicic, D. A. *J. Am. Chem. Soc.* **2004**, *126*, 8100. (f) Jones, G. D.; Martin, J. L.; McFarland, C.; Allen, O. R.; Hall, R. E.; Haley, A. D.; Brandon, R. J.; Konovalova, T.; Desrochers, P. J.; Pulay, P.; Vicic, D. A. *J. Am. Chem. Soc.* **2006**, *128*, 13175. (g) Dubinina, G. G.; Brennessel, W. W.; Miller, J. L.; Vicic, D. A. *Organometallics* **2008**, *27*, 3933. (h) Higgs, A. T.; Zinn, P. J.; Sanford, M. S. *Organometallics* **2010**, *29*, 5446. (i) Zheng, B.; Tang, F.; Luo, J.; Schultz, J. W.; Rath, N. P.; Mirica, L. M. *J. Am. Chem. Soc.* **2014**, *136*, 6499.

(8) (a) Camasso, N. M.; Sanford, M. S. *Science* **2015**, *347*, 1218. (b) Bour, J. R.; Camasso, N. M.; Sanford, M. S. *J. Am. Chem. Soc.* **2015**, *137*, 8034.

(9) (a) Lanci, M. P.; Remy, M. S.; Kaminsky, W.; Mayer, J. M.; Sanford, M. S. *J. Am. Chem. Soc.* **2009**, *131*, 15618. (b) Khusnutdinova, J. R.; Qu, F.; Zhang, Y.; Rath, N. P.; Mirica, L. M. *Organometallics* **2012**, *31*, 4627. (c) Tang, F.; Zhang, Y.; Rath, N. P.; Mirica, L. M. *Organometallics* **2012**, *31*, 6690. (d) Lotz, M. D.; Remy, M. S.; Lao, D. B.; Ariafard, A.; Yates, B. F.; Canty, A. J.; Mayer, J. M.; Sanford, M. S. *J. Am. Chem. Soc.* **2014**, *136*, 8237. (e) Wang, D.; Izawa, Y.; Stahl, S. S. *J. Am. Chem. Soc.* **2014**, *136*, 9914.

(10) Pérez-Temprano, M. H.; Casares, J. A.; Espinet, P. *Chem. - Eur. J.* **2012**, *18*, 1864.

(11) For a related mechanism with free radical intermediates, see: Bakac, A.; Espenson, J. H. *J. Am. Chem. Soc.* **1986**, *108*, 719.

(12) Kochi's attempt to characterize C−C bond formation from high-valent Ni led to the reductive elimination of Ar−PEt_3^+ from $(PEt_3)_2Ni^{III}(Ar)Br^+$: Tsou, T. T.; Kochi, J. K. *J. Am. Chem. Soc.* **1978**, *100*, 1634.

(13) (a) Yoshikai, N.; Mashima, H.; Nakamura, E. *J. Am. Chem. Soc.* **2005**, *127*, 17978. (b) Yoshikai, N.; Matsuda, H.; Nakamura, E. *J. Am. Chem. Soc.* **2009**, *131*, 9590.

(14) (a) Klappa, J. J.; Rich, A. E.; McNeill, K. *Org. Lett.* **2002**, *4*, 435. (b) Tsvetkov, N. P.; Chen, C.-H.; Andino, J. G.; Lord, R. L.; Pink, M.; Buell, R. W.; Caulton, K. G. *Inorg. Chem.* **2013**, *52*, 9511.

(15) The preference for the *trans* geometry is consistent with previous studies on d^8 square planar complexes: Fraccarollo, D.; Bertani, R.; Mozzon, M.; Belluco, U.; Michelin, R. A. *Inorg. Chim. Acta* **1992**, *201*, 15.

(16) In this rigorously dry system, the source of the protons is unclear. Control experiments reveal that **2** reacts rapidly with a trace amount of water to form methane. We were able to characterize one of the resulting Ni species to be $(py\text{-}^{Me}pyrr)_2Ni(bpy)$ **9** (Figure S3(A)).

(17) Hayduk, W. In *Solubility Data Series*; Kertes, A. S., Ed.; Pergamon: Oxford, 1982; Vol. *9*, p 138.

(18) The elevated baseline is an artifact from close *g* values for the rhombic spectrum. This effect is not pronounced in THF (Figure S6). For an example of baseline lifting due to close *g* values, see: Hearshen, D. O.; Hagen, W. R.; Sands, R. H.; Grande, H. J.; Crespi, H. L.; Gunsalus, I. C.; Dunham, W. R. *J. Magn. Reson.* **1986**, *69*, 440.

(19) Neese, F. *Wiley Interdisciplinary Reviews: Computational Molecular Science* **2012**, *2*, 73.

(20) Kinetic fitting was carried with COPASI software: Hoops, S.; Sahle, S.; Gauges, R.; Lee, C.; Pahle, J.; Simus, N.; Singhal, M.; Xu, L.; Mendes, P.; Kummer, U. *Bioinformatics* **2006**, *22*, 3067.

(21) The early points of ethane slightly deviate from the fitting. We attribute this error to imperfect shimming at the beginning of the experiments.

(22) See Supporting Information for attempted experiments to prepare (py-pyrr)Ni(halide).

(23) Nelson, I. V.; Iwamoto, R. T. *J. Electroanal. Chem.* **1964**, *7*, 218.

(24) (a) Higgs, A. T.; Zinn, P. J.; Simmons, S. J.; Sanford, M. S. *Organometallics* **2009**, *28*, 6142. (b) Renz, A. L.; Pérez, L. M.; Hall, M. B. *Organometallics* **2011**, *30*, 6365.

(25) For stable Ni(III) halide complexes, see: (a) Oguro, K.; Wada, M.; Sonoda, N. *J. Organomet. Chem.* **1979**, *165*, C10. (b) Grove, D. M.; Van Koten, G.; Zoet, R.; Murrall, N. W.; Welch, A. J. *J. Am. Chem. Soc.* **1983**, *105*, 1379. (c) Gray, L. R.; Higgins, S. J.; Levason, W.; Webster, M. *J. Chem. Soc., Dalton Trans.* **1984**, 459. (d) Grove, D. M.; Van Koten, G.; Mul, P.; Zoet, R.; Van der Linden, J. G. M.; Legters, J.; Schmitz, J. E. J.; Murrall, N. W.; Welch, A. J. *Inorg. Chem.* **1988**, *27*, 2466.

(26) (a) Klein, H.-F.; Bickelhaupt, A.; Jung, T.; Cordier, G. *Organometallics* **1994**, *13*, 2557. (b) Klein, H.-F.; Bickelhaupt, A.; Lemke, M.; Sun, H.; Brand, A.; Jung, T.; Röhr, C.; Flörke, U.; Haupt, H.-J. *Organometallics* **1997**, *16*, 668.

(27) The same effect is present in previous dimeric Ni(III) complexes: (a) Hikichi, S.; Yoshizawa, M.; Sasakura, Y.; Komatsuzaki, H.; Moro-oka, Y.; Akita, M. *Chem. - Eur. J.* **2001**, *7*, 5011. (b) Lee, C.-M.; Chiou, T.-W.; Chen, H.-H.; Chiang, C.-Y.; Kuo, T.-S.; Liaw, W.-F. *Inorg. Chem.* **2007**, *46*, 8913. (c) Kuwamura, N.; Kitano, K.; Hirotsu, M.; Nishioka, T.; Teki, Y.; Santo, R.; Ichimura, A.; Hashimoto, H.; Wright, L. J.; Kinoshita, I. *Chem. - Eur. J.* **2011**, *17*, 10708.

(28) For recent examples, see: (a) Csok, Z.; Vechorkin, O.; Harkins, S. B.; Scopelliti, R.; Hu, X. *J. Am. Chem. Soc.* **2008**, *130*, 8156. (b) Wotal, A. C.; Ribson, R. D.; Weix, D. J. *Organometallics* **2014**, *33*, 5874.

(29) Pieck, R.; Steacie, E. W. R. *Can. J. Chem.* **1955**, *33*, 1304.

(30) Fernández, I.; Trovitch, R. J.; Lobkovsky, E.; Chirik, P. J. *Organometallics* **2008**, *27*, 109.

DOI: 10.1021/jacs.6b00016
J. Am. Chem. Soc. 2016, 138, 4779−4786